Comprehensive analysis of compositional interface fluctuations in planar lipid bilayer membranes

Tao Han
Department of Mechanical and Aerospace Engineering, Princeton University, Princeton, New Jersey 08544, USA

Mikko Haataja
Department of Mechanical and Aerospace Engineering,
Princeton Institute for the Science and Technology of Materials (PRISM), and
Program in Applied and Computational Mathematics (PACM), Princeton University, Princeton, New Jersey 08544, USA

(Received 17 August 2011; revised manuscript received 22 September 2011; published 8 November 2011)

In this paper we present a comprehensive analysis of line tension-driven compositional interface fluctuations in planar lipid bilayer membranes. Our starting point is the advective Cahn-Hilliard equation for the local lipid composition in symmetric membranes, which explicitly incorporates both advective and diffusive lipid transport processes, and which is coupled to the continuum hydrodynamic equations governing the flow behavior of the membrane and surrounding solvent with finite subphase thickness. In order to extract the interface dynamics from the continuum phase-field formalism, we first derive the appropriate sharp-interface limit equations. We then carry out a linear perturbation analysis for the relaxational dynamics of small-amplitude sinusoidal interface fluctuations to yield the general dispersion relation ω_k as a function of perturbation wave number k. The resulting expression incorporates the effects of diffusive and advective lipid transport processes within the membrane, viscous or viscoelastic membrane properties, coupling between membrane and solvent, and inertial effects within the membrane and solvent. It is shown that previously considered scenarios naturally emerge as limiting cases of the general result. Furthermore, we discuss two additional scenarios amenable to analysis, one in which the inertia of the solvent is relevant, and another one in which the membrane displays significant viscoelastic properties. Finally, we numerically evaluate the general dispersion relation for three representative model membrane systems.

DOI: 10.1103/PhysRevE.84.051903 PACS number(s): 87.14.Cc, 87.15.A−, 87.16.dj

I. INTRODUCTION

Multicomponent lipid bilayer membranes comprise a class of soft materials with intriguing physical, chemical, mechanical, and biological properties. They self-assemble spontaneously in an aqueous solvent and form effectively two-dimensional (2D) surfaces embedded within the three-dimensional (3D) solvent. They are also ubiquitous in mammalian cells where, together with proteins, they facilitate the interaction of cells with their surroundings. The lipid membrane may be compositionally homogeneous or heterogeneous, and structurally (and thus mechanically) either solid-like or liquid, and even display coexistence between solid and liquid phases or multiple liquid phases with distinct lipid compositions. Experimental studies on model membrane systems have yielded a plethora of important insights into both the structure and dynamics of such compositional lipid domains in synthetic lipid vesicles [1–5].

The formation of compositional lipid microdomains and their dynamics in model membrane systems have been studied theoretically in the vicinity of second-order phase-transition points [6] and computationally below the critical point where large-scale phase separation and microdomain growth ensues [7–12]. In all, these studies have demonstrated that several domain growth mechanisms (such as lipid diffusion, advective flow, and Brownian coagulation of domains) may contribute to the overall morphology evolution at different stages during the coarsening process. Furthermore, they have also highlighted the importance of both advective flow effects within the membrane and the hydrodynamic coupling between the membrane and surrounding solvent on compositional domain formation dynamics, and some of them have even raised critical questions with regard to the validity of the dynamical scaling hypothesis for coarsening at the critical composition [12].

Once the compositional domains have formed, they display interesting compositional interface fluctuation behavior. Here thermal fluctuations give rise to undulations about a planar or circular interface ("thermal roughening"), while line tension forces provide a restoring force that limits the undulation amplitude. One of the key quantitative questions regarding such interface fluctuations is the time-dependent decay of a small sinusoidal fluctuation about a planar interface with a given wave number k; this is usually cast in the form of a k-dependent dispersion relation. As in the case of compositional domain growth and coarsening, several physical mechanisms, such as lipid diffusion and hydrodynamic flow effects, are expected to contribute to interface fluctuation dynamics.

Relevant for lipid bilayer domains, several special cases of the dispersion relation have been elucidated theoretically in previous work. These special cases range from purely 2D hydrodynamic considerations of Newtonian fluids, which ignore the coupling between the membrane and solvent [13,14], to quasi-3D treatments, which explicitly couple the 2D membrane with 3D solvent hydrodynamic flow fields in the absence of inertial effects [15–18], and, most recently, approaches that include membrane viscoelastic effects [19]. While these studies have elucidated the roles of several relevant coupling mechanisms, they have not explicitly considered the roles of diffusive lipid transport processes or solvent inertial effects. In fact, what is missing is a comprehensive treatment of compositional interface fluctuations that explicitly includes

all of the aforementioned physical processes contributing to the decay of interface fluctuations.

The goal of this manuscript is to present the derivation of a general dispersion relation that explicitly includes the effects of diffusive and advective lipid transport processes within the symmetric bilayer membrane, viscous or viscoelastic membrane properties, coupling between membrane and solvent, and inertial effects within the membrane and solvent with finite subphase thickness. In the present context, the word "symmetric" implies a bilayer membrane system for which the compositions in the two leaflets are identical, and for which the compositional phases within each leaflet are always in perfect registry. It is shown that previously considered scenarios naturally emerge as limiting cases of the general result. Furthermore, we discuss two additional scenarios amenable to analysis, one in which the inertia of the solvent is relevant, and another one in which the membrane displays significant viscoelastic properties. Finally, we numerically evaluate the general dispersion relation for three representative model membrane systems.

The rest of this manuscript is organized as follows. In Sec. II we briefly review the continuum phase-field approach employed in this work. Having formulated the governing equations, in Sec. III we first describe how to extract the compositional interface dynamics from the phase-field formalism by carrying out a so-called sharp-interface analysis, and then proceed to derive and present the general dispersion relation. Furthermore, several limiting cases of the general dispersion relation are analyzed and numerically evaluated for representative model membrane systems in Sec. III. Finally, a brief discussion and concluding remarks can be found in Sec. IV, while the derivation of the governing equations in the sharp-interface limit can be found in the Appendix.

II. THEORETICAL APPROACH

We treat the bilayer membrane as a flat sheet with infinite spatial extent and zero thickness. As illustrated in Fig. 1, within the effectively two-dimensional membrane at $z = 0$, there are two coexisting liquid phases (either viscous or viscoelastic) with identical material and transport properties such as viscosity, density, and mobility. The membrane is in contact with an aqueous solvent occupying the $0 < z < \infty$ and $-H < z < 0$ regions, while the lower solvent region in turn is in contact with a solid substrate. In the remainder of the paper, we will refer to H as the "subphase thickness." The two liquid phases are characterized by a difference in the local lipid composition. Next, we will discuss the kinetics that govern diffusive and advective lipid transport as well as coupling between the membrane and solvent hydrodynamic flow fields.

A. Order parameter kinetics: Phase-field approach

To characterize the relative concentration within symmetric binary lipid membranes, within the continuum phase-field framework we introduce a dimensionless order parameter,

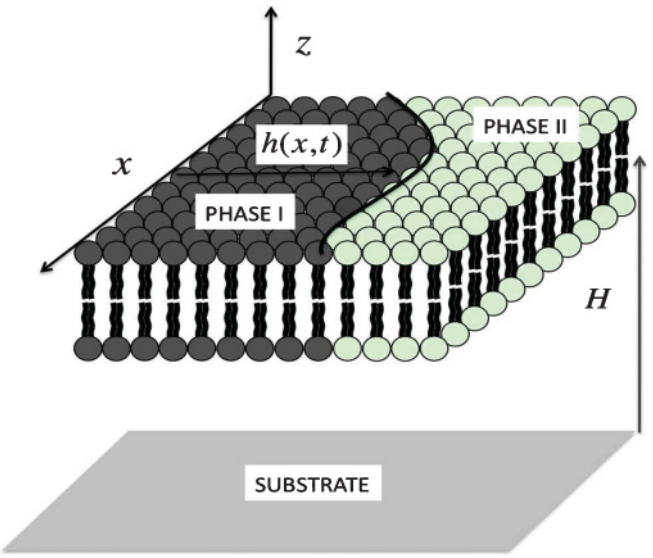

FIG. 1. (Color online) Schematic illustration of the membrane geometry. The planar membrane occupies the plane $z = 0$ with regions $0 < z < \infty$ and $-H < z < 0$ occupied by a Newtonian solvent with density ρ_S and viscosity η_S. The subphase thickness, that is, the thickness of the bottom solvent layer, is denoted by H. Within the membrane, the single-valued function $h(x,t)$ locates the compositional interface between the two phases. While the compositional interface is depicted as atomically sharp in the schematic, in reality it is diffuse with an intrinsic thickness proportional to the static correlation length ξ [20].

$\psi(\mathbf{r},t)$, which satisfies the advective Cahn-Hilliard equation [21,22]

$$\frac{\partial \psi}{\partial t} + \mathbf{u}_M \cdot \nabla \psi = M \nabla^2 \mu_\psi, \tag{1}$$

in which $\mathbf{u}_M(\mathbf{r},t)$ is the membrane velocity field, M denotes the mobility, and μ_ψ is the chemical potential defined via $\mu_\psi \equiv \delta F/\delta \psi$, where $F = \int d\mathbf{r}[W^2(\nabla\psi)^2 + f(\psi)]$ denotes a Ginzburg-Landau free-energy functional. Here the parameter W^2 is related to the mean-field line tension between the compositional phases, while f incorporates bulk thermodynamics of the binary system [20–22]. Equation (1) explicitly incorporates both diffusive and advective lipid transport phenomena and thus applies over a wide range of length scales, from the molecular to the mesoscopic regimes and beyond. Furthermore, it incorporates the presence of interfaces *implicitly*, rather than explicitly; in fact, the interfaces are located where the order parameter ψ varies rapidly yet smoothly from one compositional phase to another. Finally, it is noteworthy that Eq. (1) requires an explicit expression for the membrane velocity field $\mathbf{u}_M$ in order to evolve ψ in space and time.

B. Membrane and solvent hydrodynamics

Traditionally, the membrane has been treated as a purely viscous, two-dimensional Newtonian fluid at the continuum level. In this work we treat the membrane as a viscoelastic sheet [19,23] and assume that the membrane velocity field $\mathbf{u}_M$ satisfies the linearized viscoelastic Navier-Stokes equation

together with the incompressibility condition. That is, we consider

$$\rho_M \frac{\partial \mathbf{u}_M}{\partial t} = \int_{-\infty}^{t} G^*(t-t')\nabla^2 \mathbf{u}_M(\mathbf{r},t')\,dt' - \nabla p_M + \mathbf{f} + \mathbf{W}, \tag{2}$$

and impose

$$\nabla \cdot \mathbf{u}_M = 0. \tag{3}$$

Here p_M and ρ_M are the pressure field and density of the membrane, respectively, $\mathbf{f}$ is the effective body force exerted on the membrane by the surrounding solvent via the no-slip boundary condition, while the term $\mathbf{W}(\mathbf{r},t) = -\psi\nabla\mu_\psi$ accounts for the effect of compositional variations on the membrane stress tensor. Finally, the memory kernel $G^*(t-t')$ in Eq. (2) accounts for linear viscoelastic effects. More specifically, the off-diagonal components of the stress tensor Π_{ij} are related to strain rate tensor $\epsilon_{ij} \equiv (\partial u_{Mi}/\partial x_j + \partial u_{Mj}/\partial x_i)$ via $\hat{\Pi}_{ij}(\mathbf{r},\omega) = \hat{G}^*(\omega)\hat{\epsilon}_{ij}(\mathbf{r},\omega)$ in frequency representation, where $\hat{G}^*(\omega)$ denotes the temporal Fourier transform of $G^*(t)$.

For the solvent, we assume that it is purely viscous and satisfies the linearized Navier-Stokes equation:

$$\rho_S \frac{\partial \mathbf{u}_S}{\partial t} = \eta_S \nabla^2 \mathbf{u}_S - \nabla p_S \tag{4}$$

together with the incompressibility condition

$$\nabla \cdot \mathbf{u}_S = 0. \tag{5}$$

Here $\mathbf{u}_S$ and p_S denote the velocity and pressure of the solvent, respectively, ρ_S is the solvent density, and η_S is the dynamic solvent viscosity. Along the membrane at $z = 0$, we assume the presence of a no-slip boundary condition such that $\mathbf{u}_S(x,y,z=0,t) = \mathbf{u}_M(x,y,t)$, while $u_{Sz}(x,y,z) = 0$. Far above the membrane, we take the solvent to be quiescent, while we impose a no-slip boundary condition along the solid substrate at $z = -H$. Thus, from Eqs. (4) and (5), it follows that $\hat{\mathbf{u}}_S^+(\mathbf{q},z,\omega) = \hat{\mathbf{u}}_M(\mathbf{q},\omega)\exp(-\sqrt{q^2+\frac{i\omega\rho_S}{\eta_S}}z)$, while $\hat{\mathbf{u}}_S^-(\mathbf{q},z,\omega) = \hat{\mathbf{u}}_M(\mathbf{q},\omega)[A\exp(\sqrt{q^2+\frac{i\omega\rho_S}{\eta_S}}z) + B\exp(-\sqrt{q^2+\frac{i\omega\rho_S}{\eta_S}}z)]$, where $A = 1/[1-\exp(-2\sqrt{q^2+\frac{i\omega\rho_S}{\eta_S}}H)]$ and $B = -\exp(-2\sqrt{q^2+\frac{i\omega\rho_S}{\eta_S}}H)/[1-\exp(-2\sqrt{q^2+\frac{i\omega\rho_S}{\eta_S}}H)]$. Furthermore, $\hat{u}_{Sx}$, $\hat{u}_{Sy}$, $\hat{u}_{Mx}$, and $\hat{u}_{My}$ stand for the Fourier transforms of u_{Sx}, u_{Sy}, u_{Mx}, and u_{My} respectively, while the superscripts "+" and "−" stand for the $z > 0$ and $z < 0$ regions respectively, and $q^2 = q_1^2 + q_2^2$. Finally, the effective body force on the membrane can be written $\mathbf{f} = \lim_{z\to 0^+}\eta_S\partial\mathbf{u}_S^+/\partial z - \lim_{z\to 0^-}\eta_S\partial\mathbf{u}_S^-/\partial z$, which yields $\hat{\mathbf{f}} = -\eta_S\sqrt{q^2+\frac{i\omega\rho_S}{\eta_S}}[1+\coth(H\sqrt{q^2+\frac{i\omega\rho_S}{\eta_S}})]\hat{\mathbf{u}}_M(\mathbf{q},\omega)$ in Fourier representation.

As a consequence of the linearization of the Navier-Stokes equations in the membrane and solvent velocity fields, they admit explicit solutions. In particular, solving Eqs. (2) and (3) in Fourier space and imposing the no-slip boundary condition along the membrane yields

$$\hat{\mathbf{u}}_M(\mathbf{q},\omega) = \hat{\mathbf{T}}(\mathbf{q},\omega)\cdot\hat{\mathbf{W}}(\mathbf{q},\omega), \tag{6}$$

where $\hat{\mathbf{W}}(\mathbf{q},\omega)$ denotes the Fourier transform of the vector $\mathbf{W}(\mathbf{r},t) = -\psi\nabla\mu_\psi$, and the modified Oseen tensor

$$\hat{T}_{\alpha\beta}(\mathbf{q},\omega) = \frac{1}{i\rho_M\omega + q^2\hat{G}^*(\omega) + \eta_S\sqrt{q^2+\frac{i\omega\rho_S}{\eta_S}}\left[1+\coth\left(H\sqrt{q^2+\frac{i\omega\rho_S}{\eta_S}}\right)\right]}\left(\delta_{\alpha\beta} - \frac{q_\alpha q_\beta}{q^2}\right) \tag{7}$$

with $q^2 = q_1^2 + q_2^2$. Note that the modified Oseen tensor $\hat{\mathbf{T}}$ explicitly incorporates inertial and viscous effects within the solvent and finite subphase thickness, as well as inertial and viscoelastic effects within the membrane. In the limit $H \to \infty$, $\hat{\mathbf{T}}$ reduces to a form very recently derived by Camley and Brown [19]. In the purely viscous membrane limit $\hat{G}^*(\omega) = \eta_M$, it also reduces to the form obtained previously by Serra and Rubí [24] when $H \to \infty$, and Lubensky and Goldstein [25] and Oppenheimer and Diamant [26] for finite H and $\rho_M = \rho_S = 0$. It is noteworthy that, in the context of lipid bilayer membranes, the above equations in the overdamped viscous limit have been previously employed to investigate collective dynamics near a critical point [6] and spinodal decomposition kinetics below the critical point in the presence [11] and absence [12] of thermal fluctuations.

C. Sharp interface limit analysis: From phase fields to effective interface equations

Having formulated the governing equations within the phase-field formalism, we now turn to the problem of how to extract the compositional interface dynamics from Eq. (1). The challenge here is that the phase-field approach incorporates the presence of interfaces *implicitly*, rather than explicitly. In fact, the interfaces are located where the order parameter ψ varies rapidly yet smoothly over a length scale proportional to the equilibrium correlation length ξ from one compositional phase to another. To this end, we will extract the interfacial dynamics by carrying out a so-called sharp-interface analysis. The basic qualitative idea is as follows. We consider solutions to the governing equations in two distinct spatial regions, namely, regions in the vicinity of an interface ("inner region") and away from any interfaces ("outer region"). The governing equations in the outer region reduce to bulk equations, while matching the outer solutions to the inner ones provides the appropriate boundary conditions on the interface in the sharp-interface limit.

Technically this procedure is carried out by means of matched asymptotic expansions, in which the small expansion parameter ϵ is related to the intrinsic interfacial width ξ and the velocity normal to the interface v_c via $\epsilon = \kappa_c\xi \sim \xi v_c/D_\psi$, where D_ψ and κ_c denote the collective lipid diffusion coefficient and characteristic curvature of the interface, respectively. Physically, the restriction $\epsilon \ll 1$ implies both that the interface

is gently curved on the scale of the intrinsic interface width and that the normal velocity of the interface is sufficiently small to admit effectively instantaneous relaxation of the order parameter diffusion field within the interface. In other words, the system is only slightly perturbed away from thermodynamic equilibrium.

In order to derive the sharp-interface limit equations, we make extensive use of the asymptotic analysis procedure developed by Elder *et al*. [20] for a class of phase-field models that are purely diffusive (and thus do not include advective terms). Including the advective term in the procedure is, in fact, straightforward. As shown in the Appendix, the governing equation now becomes an advection-diffusion equation within the bulk phases:

$$\frac{\partial \delta\psi}{\partial t} + \mathbf{u}_M \cdot \nabla \delta\psi = D_\psi \nabla^2 \delta\psi. \tag{8}$$

Here $\delta\psi = \psi - \psi_{\rm eq}^{\pm}$ denotes the deviation of the order parameter from its local bulk equilibrium value, while the diffusivity is related to the mobility M and equilibrium chemical potential via $D_\psi \equiv M \frac{\partial \mu_\psi}{\partial \psi}|_{\psi_{\rm eq}}$. As in the purely diffusive case (corresponding to $\mathbf{u}_M = 0$), solving the perturbative equations in the inner region and matching them to the outer solutions provides the two boundary conditions specified along the moving interface. The analysis outlined in the Appendix demonstrates that these boundary conditions are in turn given by

$$\frac{\delta\psi_{\rm int}}{\Delta\psi_{\rm eq}} = -d_0\kappa \tag{9}$$

and

$$v_n|_{\rm int} = u_{Mn}|_{\rm int} + \frac{1}{\Delta\psi_{\rm eq}}[D_\psi \nabla\delta\psi \cdot \mathbf{n}]_{0^+}^{0^-}, \tag{10}$$

where $\delta\psi_{\rm int} = \psi|_{\rm int} - \psi_{\rm eq}^{\pm}$ denotes the local excess order parameter along the interface, and d_0, κ, $v_n|_{\rm int}$, $u_M|_{\rm int}$, and $\mathbf{n}$ denote the capillary length, local curvature of the interface, the normal component of interface velocity, membrane velocity normal to the interface, and unit vector normal to the interface, respectively, and where the equilibrium miscibility gap is given by $\Delta\psi_{\rm eq} = \psi_{\rm eq}^{+} - \psi_{\rm eq}^{-}$. Furthermore, the notation $[X]_{0^+}^{0^-} \equiv X(0^-) - X(0^+)$ denotes the jump in the quantity "X" across the interface. Equation (9) is the standard Gibbs-Thomson boundary condition for equilibrium along curved interfaces, while Eq. (10) simply states that the compositional interface relaxes by both advection as dictated by the local membrane flow velocity as well as by lipid diffusion.

Finally, for the hydrodynamic equations, the equations themselves do not change in the sharp interface limit; the only change is the form of the source term $\mathbf{W}(\mathbf{r},t) = -\psi\nabla\mu_\psi$. According to Ref. [21], $\mathbf{W}$ can be expressed as

$$\mathbf{W}(\mathbf{r},t) = \sigma\kappa\mathbf{n}\delta(\mathbf{r} - \mathbf{r_s}) \tag{11}$$

in the sharp interface limit, where $\mathbf{r_s}$ is the instantaneous location of the interface and σ is the interfacial tension, taken to be constant in this work. [In passing, we note that d_0 and σ are not independent parameters within the phase-field approach. In fact, as shown in Ref. [20], $d_0 = \sigma/[(\Delta\psi_{\rm eq})^2 \partial\mu_\psi/\partial\psi|_{\psi_{\rm eq}}]$, while $\sigma = W^2 \int_{-\infty}^{\infty} du (\partial\psi_0^{\rm in}/\partial u)^2$, with $\psi_0^{\rm in}(u)$ denoting the zeroth-order, equilibrium solution in the inner region.] Thus, the membrane velocity field still satisfies Eq. (6) with $\hat{\mathbf{W}}(\mathbf{q},\omega)$ now denoting the Fourier transform of the vector $\mathbf{W}(\mathbf{r},t) = \sigma\kappa\mathbf{n}\delta(\mathbf{r} - \mathbf{r_s})$. To summarize, the governing equations in the sharp-interface limit are (a) Eq. (8) for the order parameter dynamics within bulk phases, (b) Eqs. (6), (7), and (11) for the membrane velocity field $\mathbf{u}_M$, and (c) Eqs. (9) and (10) as boundary conditions to be enforced along the moving interface. These equations provide the starting point for a comprehensive analysis of compositional interface fluctuations across a wide range of length and time scales, to which we turn next.

III. COMPOSITIONAL INTERFACE FLUCTUATIONS

In this section we will first derive an analytical expression for the general dispersion relation. Then we will analyze the dispersion relation for several limiting cases. Finally, we will evaluate the dispersion relation numerically for three representative model membrane systems.

A. Derivation of the general dispersion relation

In this part we will derive the general dispersion relation, which governs the relaxation dynamics of sinusoidal interface fluctuations around a planar interface. The analysis proceeds as follows. First, we assume that the morphology of the interface can be expressed as $h(x,t) = h_0 \exp(i\omega_k t + ikx) + \text{c.c}$, where "c.c" denotes complex conjugation, and the perturbation amplitude h_0 is taken to be infinitesimal such that $hk \ll 1$ at all times. The goal of the calculation is to obtain the (generally) complex-valued ω_k as a function of the perturbation wave number k.

In order to proceed further, we look for solutions for $\mathbf{u}_M$ of the form $\mathbf{u}_M(x,y,t) = \mathbf{p}(y;k,\omega_k)\exp(i\omega_k t + ikx)$. Upon substituting this ansatz in Eq. (2), Fourier transforming in y, and imposing the incompressibility condition, we obtain

$$\begin{bmatrix} \hat{p}_x(q_2;k,\omega_k) \\ \hat{p}_y(q_2;k,\omega_k) \end{bmatrix} = \hat{\mathbf{T}}(k,q_2,\omega_k) \cdot \begin{bmatrix} 0 \\ -\sigma k^2 h_0 \end{bmatrix}, \tag{12}$$

or

$$\begin{bmatrix} \hat{p}_x(q_2;k,\omega_k) \\ \hat{p}_y(q_2;k,\omega_k) \end{bmatrix} = -\frac{\sigma k^2 h_0}{i\rho_M\omega_k + \bar{q}^2\hat{G}^*(\omega_k) + \eta_S\sqrt{\bar{q}^2 + \frac{i\omega_k\rho_S}{\eta_S}}\left[1 + \coth\left(H\sqrt{\bar{q}^2 + \frac{i\omega_k\rho_S}{\eta_S}}\right)\right]} \begin{bmatrix} -kq_2/\bar{q}^2 \\ k^2/\bar{q}^2 \end{bmatrix}, \tag{13}$$

where $\bar{q}^2 = k^2 + q_2^2$ and $\hat{\mathbf{T}}$ is the Oseen tensor from Eq. (7). In arriving at these expressions, we have made use of the fact that $\kappa \approx \partial^2 h/\partial x^2$ and $\mathbf{n} \approx [0,1]^T$, implying that $\mathbf{W}(\mathbf{r},t) \approx [0, -\sigma k^2 h\delta(y)]^T$ to leading order in h. In passing, we note that these manipulations require that $G^*(t)$ decays sufficiently rapidly when $t \to \infty$ such that integrals of the form $\int_0^\infty dt G^*(t)\exp(-i\omega_k t)$ converge for complex-valued ω_k. Hence, upon carrying out an inverse Fourier transform in y, we

obtain

$$\begin{bmatrix} u_{Mx}(x,y,t) \\ u_{My}(x,y,t) \end{bmatrix} = -\frac{1}{2\pi}\int_{-\infty}^{\infty} dq_2 \frac{\sigma k^2 h_0 \exp(i\omega_k t + ikx + iq_2 y)}{i\rho_M\omega_k + \bar{q}^2\hat{G}^*(\omega_k) + \eta_S\sqrt{\bar{q}^2 + \frac{i\omega_k\rho_S}{\eta_S}}\left[1+\coth\left(H\sqrt{\bar{q}^2+\frac{i\omega_k\rho_S}{\eta_S}}\right)\right]} \begin{bmatrix} -kq_2/\bar{q}^2 \\ k^2/\bar{q}^2 \end{bmatrix}. \quad (14)$$

Evaluating the expressions above at the interface $y = h(x,t)$, yields, to first order in h,

$$\begin{bmatrix} u_{Mx}(x,t)_{\rm int} \\ u_{My}(x,t)_{\rm int} \end{bmatrix} = -\frac{1}{2\pi}\int_{-\infty}^{\infty} dq_2 \frac{\sigma k^2 h_0 \exp(i\omega_k t + ikx)}{i\rho_M\omega_k + \bar{q}^2\hat{G}^*(\omega_k) + \eta_S\sqrt{\bar{q}^2 + \frac{i\omega_k\rho_S}{\eta_S}}\left[1+\coth\left(H\sqrt{\bar{q}^2+\frac{i\omega_k\rho_S}{\eta_S}}\right)\right]} \begin{bmatrix} -kq_2/\bar{q}^2 \\ k^2/\bar{q}^2 \end{bmatrix}, \quad (15)$$

or

$$\begin{bmatrix} u_{Mx}(x,t)_{\rm int} \\ u_{My}(x,t)_{\rm int} \end{bmatrix} = \begin{bmatrix} \frac{\sigma k^3 h}{2\pi}\int_{-\infty}^{\infty} \frac{\tilde{q}\,d\tilde{q}}{(a_M+a_S)(1+\tilde{q}^2)} \\ -\frac{\sigma k^3 h}{2\pi}\int_{-\infty}^{\infty} \frac{d\tilde{q}}{(a_M+a_S)(1+\tilde{q}^2)} \end{bmatrix}, \quad (16)$$

where

$$a_M \equiv i\rho_M\omega_k + k^2\hat{G}^*(\omega_k)(1+\tilde{q}^2) \quad (17)$$

and

$$a_S \equiv \eta_S\sqrt{k^2(1+\tilde{q}^2)+\frac{i\omega_k\rho_S}{\eta_S}} \times\left[1+\coth\left(H\sqrt{k^2(1+\tilde{q}^2)+\frac{i\omega_k\rho_S}{\eta_S}}\right)\right]. \quad (18)$$

Now, as given by the kinematic boundary condition in Eq. (10), to first order in h, the normal interface velocity can be written

$$v_n|_{\rm int} = \frac{\partial h(x,t)}{\partial t} = i\omega_k h = u_{My}|_{\rm int} + \frac{1}{\Delta\psi_{\rm eq}}[D_\psi\nabla\delta\psi\cdot\mathbf{n}]_{0^+}^{0^-}, \quad (19)$$

or

$$i\omega_k h = -\frac{\sigma k^3 h}{2\pi}\int_{-\infty}^{\infty}\frac{d\tilde{q}}{(a_M+a_S)(1+\tilde{q}^2)} + \frac{1}{\Delta\psi_{\rm eq}}[D_\psi\nabla\delta\psi\cdot\mathbf{n}]_{0^+}^{0^-}. \quad (20)$$

Next, the contribution of diffusive lipid transport to the interfacial velocity (i.e., the second term in the expression above) can be obtained by solving the bulk equation (8), imposing the Gibbs-Thomson boundary condition Eq. (9), and linearizing the resulting expression in h to yield

$$\frac{1}{\Delta\psi_{\rm eq}}[D_\psi\nabla\delta\psi\cdot\mathbf{n}]_{0^+}^{0^-} \approx -2k^3 h d_0 D_\psi. \quad (21)$$

Finally, combining the results from Eqs. (20) and (21) yields the general dispersion relation for small-amplitude fluctuations about a planar interface, given by

$$i\omega_k = -\frac{\sigma k^3}{2\pi}\int_{-\infty}^{\infty}\frac{d\tilde{q}}{(a_M+a_S)(1+\tilde{q}^2)} - 2k^3 d_0 D_\psi, \quad (22)$$

where a_M and a_S are displayed in Eqs. (17) and (18), respectively.

Equation (22) is the central result of this paper. It quantifies the roles of not only the viscous and inertial hydrodynamic effects from both the solvent and the membrane on the interface dynamics, but also diffusive effects at short distances as well as viscoelastic behavior of the bilayer membrane, and incorporates a finite subphase thickness. The expression in Eq. (22) is rather complex, and in order to illustrate its salient features, we will first examine its implications in specific limits. In particular, we demonstrate that existing theoretical results are contained in it as special cases. Then, we identify two new regimes, namely, a 2D viscoelastic regime in which the viscoelastic properties of the membrane dominate, and a 3D inertial regime, in which the inertia of the solvent dominates the fluctuation dynamics. Finally, we numerically evaluate the full dispersion relation for three representative model membrane systems.

B. Limiting cases of the general dispersion relation

Let us next demonstrate that the known limits emerge naturally from the general expression in Eq. (22). In particular, these limits correspond to diffusion dominated, 2D membrane flow dominated, and viscous quasi-3D solvent dominated regimes, respectively. In addition, we will further demonstrate the emergence of two new regimes arising from viscoelastic nature of the membrane in the quasi-2D case and inertial effects in the quasi-3D case in the infinitely thick subphase limit.

1. Diffusion-dominated

The first limiting case corresponds to diffusion-dominated lipid transport at short length scales. Upon ignoring advective lipid transport effects, the dispersion reduces to the well-known [20] result $\omega_k^{\rm diff} = i2k^3 d_0 D_\psi = i2k^3\sigma M/(\Delta\psi_{\rm eq})^2$. In this limit, diffusion is very effective in relaxing interface fluctuations at molecular length scales, while at longer scales it becomes very inefficient due to the $|\omega_k^{\rm diff}| \sim k^3$ scaling.

2. Purely 2D membrane in absence of diffusive transport

The second limiting case is a purely 2D membrane decoupled from the solvent and in the absence of diffusive lipid transport effects. Upon setting $D_\psi = 0$ and $\eta_S = 0$, we obtain

$$i\omega_k = -\frac{\sigma k^3}{2\pi}\int_{-\infty}^{\infty}\frac{d\tilde{q}}{(1+\tilde{q}^2)[i\rho_M\omega_k + \hat{G}^*(\omega_k)k^2(1+\tilde{q}^2)]}. \quad (23)$$

Carrying out the integration yields

$$i\omega_k = -\frac{\sigma k^3}{2\rho_M i\omega_k}\left[1-\sqrt{\frac{\hat{G}^*(\omega_k)k^2}{\hat{G}^*(\omega_k)k^2 + i\rho_M\omega_k}}\right]. \quad (24)$$

In the overdamped limit ($\hat{G}^*(\omega_k)k^2 \gg \rho_M|\omega_k|$), we readily obtain

$$\omega_k^{\text{visc}} = \frac{i\sigma k}{4\hat{G}^*(\omega_k)}. \tag{25}$$

On the other hand, in the inertia-dominated regime ($\hat{G}^*(\omega_k)k^2 \ll \rho_M|\omega_k|$), we obtain $\omega_k^{\text{inertia}} = \pm\sqrt{\frac{\sigma}{2\rho_M}}k^{\frac{3}{2}}$, corresponding to a pair of propagating waves without damping, in agreement with Refs. [13,14]. For a Newtonian fluid with viscosity $\hat{G}^*(\omega_k) = \eta_M$, Eq. (25) reduces to purely exponential decay of fluctuations with $\omega_k^{\text{visc}} = i\sigma k/(4\eta_M)$, a result also obtained previously in Refs. [13,14]. We note that the interface Peclet number Pe, quantifying the importance of viscous transport effects relative to a diffusive one in relaxational interface fluctuations, can be written $\text{Pe} = \omega_k^{\text{visc}}/\omega_k^{\text{diff}} = \sigma/(8k^2 d_0 D_\psi \eta_M)$. The crossover from diffusion-dominated relaxational dynamics ($\text{Pe} \ll 1$) to viscous flow-dominated ($\text{Pe} \gg 1$) occurs for $\text{Pe} \sim 1$, or $k^* \sim [\sigma/(8d_0\eta_M D_\psi)]^{1/2}$. For a typical membrane with $\sigma \approx 10^{-12}$ N, $d_0 \approx 10^{-8}$ m, $\eta_M \approx 10^{-9}$ Pa s m, and $D_\psi \approx 10^{-12}$ m^2/s, the crossover occurs at $k^* \approx 10^8$ m^{-1}.

3. Viscous quasi-3D without inertia and diffusion

Next, we will consider the viscous quasi-3D case, in which the membrane is coupled to the solvent with infinite subphase thickness, and both inertial and viscoelastic effects are ignored [15–18]. More specifically, we set $\rho_S = \rho_M = 0$, $\hat{G}^*(\omega_k) = \eta_M$, and $D_\psi = 0$ in Eq. (22). In this case,

$$\omega_k^{\text{visc}} = \frac{i\sigma k^3}{2\pi}\int_{-\infty}^{\infty} \frac{d\tilde{q}}{(1+\tilde{q}^2)[\eta_M k^2(1+\tilde{q}^2) + 2\eta_S k\sqrt{1+\tilde{q}^2}]}. \tag{26}$$

To further simplify, we readily obtain the well-known results $\omega_k^{\text{visc}} \approx i\sigma k/(4\eta_M)$ when $k\ell_H \gg 1$ and $\omega_k^{\text{visc}} \approx i\sigma k^2/(2\pi\eta_S)$ when $k\ell_H \ll 1$ [15–18], where we have defined the hydrodynamic length $\ell_H \equiv \eta_M/\eta_S$. In both cases the fluctuations display pure exponential decay in time. We also note that, in the case of finite subphase thickness H, $\omega_k^{\text{visc}} \approx i\sigma k^3 H/(2\eta_S)$ when $k \to 0$. As elaborated by Stone and Ajdari [27] and, very recently, by Seki *et al.* [28], this behavior can be understood on dimensional grounds by balancing the frictional force on the membrane $f \sim \eta_S u_M/H$ with the line tension force $\sim\sigma/L^2$ leading to $\omega_k \sim u_M/L \sim H\sigma/(\eta_S L^3)$, where $L = 2\pi/k$.

4. Viscoelastic membrane decoupled from solvent

In the following, we will focus on an intriguing regime, namely, the scenario in which the membrane viscoelastic properties dominate the fluctuation dynamics [19]. Herein, we specialize the analysis for a simple Maxwell model. For the Maxwell model, $\hat{G}^*(\omega) = \hat{G}_M^*(\omega) = \eta_M/(1+i\tau\omega)$, where η_M is the dynamic viscosity, and τ is the (elastic) relaxation time, so that $G_M^*(t) = \frac{\eta_M}{\tau}\exp(-\frac{t}{\tau})u(t)$, where $u(t)$ is the Heaviside unit step function. In the high-frequency limit $\tau\omega \gg 1$, the membrane responds elastically with an effective shear modulus η_M/τ, while in the low-frequency limit $\tau\omega \ll 1$, the membrane is viscous with a viscosity given by η_M. In the quasi-2D viscoelastic case ($\rho_M = 0$, $\eta_S = 0$ and $D_\psi = 0$), Eq. (25) implies

$$\omega_k^{\text{viscoel}} = \frac{i\sigma k}{4\eta_M + \sigma k\tau}. \tag{27}$$

As noted earlier by Camley and Brown [19] for the circular domain case, a finite elastic relaxation time τ effectively reduces the relaxation rate relative to the purely viscous case $\tau = 0$ at fixed viscosity. Furthermore, in the limit $\sigma k\tau/\eta_M \gg 1$, $\omega_k^{\text{viscoel}} \approx i\tau^{-1}$; that is, the relaxation rate is independent of line tension σ, viscosity η_M, and wave number k. We also note that, for the Maxwell model, $\text{Re}\{1+i\tau\omega_k\} > 0$ is required for the term $\int_{-\infty}^{t} G^*(t-t')\nabla^2\mathbf{u}_M(\mathbf{r},t')\,dt' = \frac{\eta_M}{\tau}\nabla^2[\mathbf{p}(y;k,\omega_k)\exp(ikx)]\int_{-\infty}^{t}\exp(-\frac{t-t'}{\tau})\exp(i\omega_k t')\,dt'$ in Eq. (2) to converge.

5. Solvent inertia-dominated

Finally, we consider another unconventional regime, which is the solvent inertia-dominated quasi-3D case with infinite subphase thickness, and for which the dispersion relation is determined from

$$i\omega_k = -\frac{\sigma k^3}{4\pi\eta_S}\int_{-\infty}^{\infty}\frac{d\tilde{q}}{(1+\tilde{q}^2)\sqrt{k^2(1+\tilde{q}^2) + \frac{i\omega_k\rho_S}{\eta_S}}}. \tag{28}$$

In the inertia-dominated limit $\eta_S \to 0$, $k^2(1+\tilde{q}^2) \ll |\omega_k|\rho_S/\eta_S$, we obtain

$$\omega_k^{\text{inertia}} = \left(\pm\frac{\sqrt{3}}{2} + \frac{i}{2}\right)\frac{\sigma^{2/3}k^2}{(16\rho_S\eta_S)^{1/3}}. \tag{29}$$

Interestingly, in this limit, the interface fluctuations are damped at all wave numbers k. More specifically, the ratio $\text{Re}(\omega_k)/\text{Im}(\omega_k) = \sqrt{3}$ is independent of k, which implies that all fluctuation modes decay at a rate proportional to the propagation rate. This should be contrasted with standard capillary wave fluctuations, for which $\text{Re}(\omega_k)/\text{Im}(\omega_k) \to \infty$ as $k \to 0$, implying the presence of propagating waves whose damping asymptotically vanishes. This relaxation mode becomes relevant for systems for which $\sigma\rho_S/\eta_S^2 \gg 1$, which implies line tensions of order 10^{-9} N or higher, given that $\eta_S = 10^{-3}$ Ns/m^2 and $\rho_S = 10^3$ kg/m^3 for water. While $\sigma \sim 10^{-12}$ N for typical lipid membranes [29], implying that solvent inertia effects are unimportant, it may be possible to observe such solvent inertia effects in polymeric bilayer membranes where the line tension can be tuned more readily. For convenience, the results from the specific limiting cases are summarized in Table I.

C. Model membranes: Numerical evaluation of ω_k

Having elucidated several analytically derivable limiting cases of the general dispersion relation, we now turn to representative model membrane systems, in which several kinetic relaxation mechanisms compete, in order to illustrate the relaxation of compositional fluctuations over a wide range of length and time scales. Given the complexity of the dispersion relation in Eq. (22), we resort to numerical means to evaluate it for specific model systems. To this end, we employ the generalized Newton method for nonlinear equations [30] to extract ω_k as a function of the wave number

TABLE I. Distinct limiting cases of the general dispersion relation in Eq. (22) emerging from various combinations of physical lipid transport and dissipation mechanisms. Here η_M (η_S) and ρ_M (ρ_S) denote the viscosity and density of the membrane (solvent), respectively, while D_ψ, τ, and ω_k denote the lipid diffusivity, elastic membrane relaxation time, and dispersion, respectively.

Case	η_M	ρ_M	η_S	ρ_S	D_ψ	τ	Re(ω_k)	Im(ω_k)
Diffusive [20]	0	0	0	0	Finite	0	0	$2k^3 d_0 D_\psi$
2D overdamped [13,14]	Finite	0	0	0	0	0	0	$\frac{\sigma k}{4\eta_M}$
2D inertia-dominated [13,14]	0	Finite	0	0	0	0	$\pm\sqrt{\frac{\sigma}{2\rho_M}}k^{\frac{3}{2}}$	0
Quasi-3D overdamped [15–18]	Finite	0	Finite	0	0	0	0	$\frac{\sigma k}{4\eta_M}$; $k\ell_H \gg 1$ $\frac{\sigma k^2}{2\pi\eta_S}$; $k\ell_H \ll 1$
2D viscoelastic	Finite	0	0	0	0	Finite	0	$\frac{\sigma k}{4\eta_M\left(1+\frac{\sigma k\tau}{4\eta_M}\right)}$
Quasi-3D inertia-dominated	0	0	Finite	Finite	0	0	$\pm\frac{\sqrt{3}\sigma^{2/3}k^2}{2(16\rho_S\eta_S)^{1/3}}$	$\frac{\sigma^{2/3}k^2}{2(16\rho_S\eta_S)^{1/3}}$

k. The numerical calculation proceeds as follows. First, let $i\omega_k = x + iy$. Upon substituting this expression in Eq. (22), it can be manipulated into a form $f_1(x,y) + if_2(x,y) = 0$, where f_1 and f_2 are two real-valued, nonlinear functions. To find the roots of this equation iteratively at fixed k, we start with an initial guess $\mathbf{x}_0 = [x_0, y_0]^T$. Then, we employ the iterative scheme $J_F(\mathbf{x}_n)\cdot(\mathbf{x}_{n+1} - \mathbf{x}_n) = -\mathbf{F}(\mathbf{x}_n)$, where $\mathbf{F} = [f_1, f_2]^T$ and J_F denotes the Jacobian matrix $d\mathbf{F}/d\mathbf{x}$. These equations are iterated until the solutions converge; in this work, the iterations are carried out until $|\frac{\Delta x_n}{x_n}| < \epsilon^*$ and $|\frac{\Delta y_n}{y_n}| < \epsilon^*$, where $\epsilon^* = 10^{-4}$. We verified that this convergence criterion was sufficient to provide an excellent match between numerical and analytical results for the limiting cases discussed above. Carrying out this procedure for a broad range of k values, we can obtain both real and imaginary values of ω_k as a function of k.

The numerical procedure outlined above was applied to three representative model membrane systems with infinite subphase thickness, namely, (1) a purely viscous lipid bilayer in contact with an aqueous solvent, (2) purely viscous bilayer in contact with a fictitious, low-viscosity solvent, and (3) viscoelastic membrane in contact with an aqueous solvent. The parameter values employed for the three cases are listed in Table II.

1. *Viscous lipid membrane-aqueous solvent system*

For this system we treat the lipid membrane as a pure viscous membrane, and choose water as the 3D solvent outside. The numerically obtained data for real and imaginary parts of ω_k versus k are displayed in Fig. 2. It can be seen that for all k values studied, only the imaginary part is nonzero, implying purely exponential decay of fluctuations. That is, the system is overdamped for all k. Furthermore, as expected, Im(ω_k) changes from $\sim k^2$ to $\sim k$ corresponding to the change from solvent viscosity-dominated to membrane viscosity-dominated as k increases. For this particular choice of parameters, the crossover occurs around $k^* \approx 10^6/\text{m} = 1/\ell_H$. Finally, Im($\omega_k$) starts to increase more rapidly around $k = 10^7/\text{m}$ due to diffusion effects, which become dominant at small length scales $\sim d_0$.

2. *Viscous lipid membrane-fictitious solvent system*

To bring in the effect of solvent inertia, we next focus on a purely viscous membrane system in contact with a fictitious solvent with the density of water but a much reduced viscosity. For this system, the data for real and imaginary parts of ω_k versus k are displayed in Fig. 3. It can be seen that when $k < 10^4/\text{m}$, both Re(ω_k) and Im(ω_k) are of the same order and scale as k^2, as expected from the analysis of the corresponding limiting case. It can also be seen that, when $10^5/\text{m} < k < 10^7/\text{m}$, Im($\omega_k$) $\sim k$ while Re(ω_k) ≈ 0, implying that the system becomes overdamped courtesy of viscous dissipation within the membrane, and when $k > 10^7/\text{m}$, Im(ω_k) starts to increase more rapidly due to diffusion effects. As discussed in the analysis part in Sec. III B 5, while this scenario is not expected to be relevant for lipid bilayers due to low line tension, it should be more readily observable in the case of polymeric bilayer membranes.

TABLE II. Representative parameter values corresponding to the three model membrane systems studied numerically. Here η_M (η_S) and ρ_M (ρ_S) denote the viscosity and density of the membrane (solvent), respectively, while D_ψ, τ, d_0, and σ denote the lipid diffusivity, elastic membrane relaxation time, capillary length, and interfacial line tension, respectively. Case 1 corresponds to a viscous bilayer in contact with an aqueous solvent, while case 2 corresponds to a viscous bilayer in contact with a fictitious solvent characterized by low viscosity. Finally, case 3 corresponds to a viscoelastic bilayer system in contact with an aqueous solvent.

Model system	η_M	ρ_M	η_S	ρ_S	D_ψ	d_0	τ	σ
1	10^{-9} Pa s m	10^{-6} kg/m^2	10^{-3} Pa s	10^3 kg/m^3	10^{-12} m^2/s	10^{-8} m	0	10^{-12} N
2	10^{-9} Pa s m	10^{-6} kg/m^2	10^{-6} Pa s	10^3 kg/m^3	10^{-12} m^2/s	10^{-8} m	0	10^{-12} N
3	10^{-5} Pa s m	10^{-6} kg/m^2	10^{-3} Pa s	10^3 kg/m^3	10^{-16} m^2/s	10^{-8} m	10^{-2} s	10^{-12} N

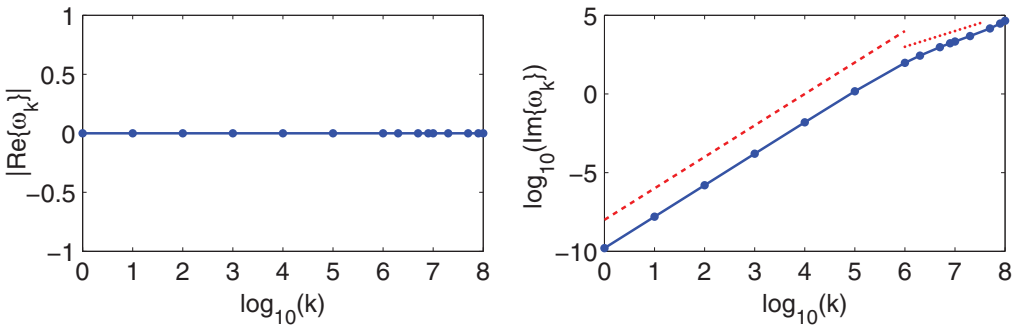

FIG. 2. (Color online) Real (left panel) and imaginary (right panel) parts of ω_k vs k for the purely viscous lipid membrane-aqueous solvent system. We note that ω_k is measured in s^{-1} while k is measured in m^{-1}. The dashed and dotted lines have slopes 2 and 1, respectively, and are guides to the eye. For this case, ω_k is pure imaginary, and thus fluctuations decay in time in a simple exponential fashion. As expected, dissipation within the solvent dominates the fluctuation relaxation rate in the limit $k \to 0$ with $\mathrm{Im}(\omega_k) \sim k^2$, while viscous dissipation within the membrane and diffusive lipid transport effects compete at large k. Here an intermediate scaling regime due to viscous dissipation within the membrane $\mathrm{Im}(\omega_k) \sim k$ is eventually replaced by the diffusive $\mathrm{Im}(\omega_k) \sim k^3$ regime at sufficiently large k.

3. *Viscoelastic lipid membrane-aqueous solvent system*

Finally, we consider a membrane system that displays significant viscoelastic behavior. We employ a Maxwell model to describe the viscoelastic behavior of the membrane, and couple the membrane to a purely viscous, aqueous solvent. Compared to the other two model membrane systems, here we consider a lipid diffusivity that is much smaller in order to reflect the viscoelastic nature of the system. For this system, the data for real and imaginary parts of ω_k versus k are displayed in Fig. 4. It can be seen that $\mathrm{Re}(\omega_k) = 0$ for all k values studied here, implying that the system is always overdamped. Furthermore, $\mathrm{Im}(\omega_k) \sim k^2$ in the solvent-dominated regime at small k and switches over to $\mathrm{Im}(\omega_k) \sim k$ at $k^* \approx 10^2/\mathrm{m}$ once dissipation within the membrane becomes important, and when $k > 10^7/\mathrm{m}$, $\mathrm{Im}(\omega_k)$ starts to increase more rapidly due to diffusion effects. As perhaps the most important observation for this case, the fluctuation relaxation rate is dominated by membrane viscoelastic properties over an extended range of k values for this choice of parameter values. Finally, we note that when $k \leqslant \frac{1}{d_0} = 10^8\ \mathrm{m}^{-1}$, the self-consistency condition $\mathrm{Re}\{1 + i\omega_k\tau\} > 0$ discussed in Sec. III B 4, is always satisfied.

4. *Comparison of fluctuation behavior in three model membrane systems*

Let us now compare and contrast the behavior of ω_k for the three representative model membrane systems. At sufficiently large k values, $\mathrm{Re}(\omega_k) = 0$ for all three systems, implying that fluctuation relaxation is always overdamped, courtesy of viscous and diffusive dissipation within the membrane. In fact, overdamped behavior is always found for all k except in the inertia-dominated case at small k. As discussed above, while this regime is not relevant for lipid membranes, it should be observable in polymeric membranes. In the cases of viscous and viscoelastic membranes in contact with an aqueous solvent, the behavior of $\omega_k \sim k^2$ in the limit $k \to 0$ is identical due to the dominance of dissipation within the solvent, while in the opposite limit $k \to 1/d_0$, diffusion eventually dominates leading to similar scaling behavior ($\omega_k \sim k^3$) in both cases. Finally, in the intermediate regime, the viscoelastic properties of the membrane dominate, leading to $\omega_k \sim k$ scaling behavior. It is noteworthy that in the viscoelastic case, when the relaxation time is macroscopic, $\omega_k \sim k$ scaling is observed over an extended range of k values, as shown in Fig. 4.

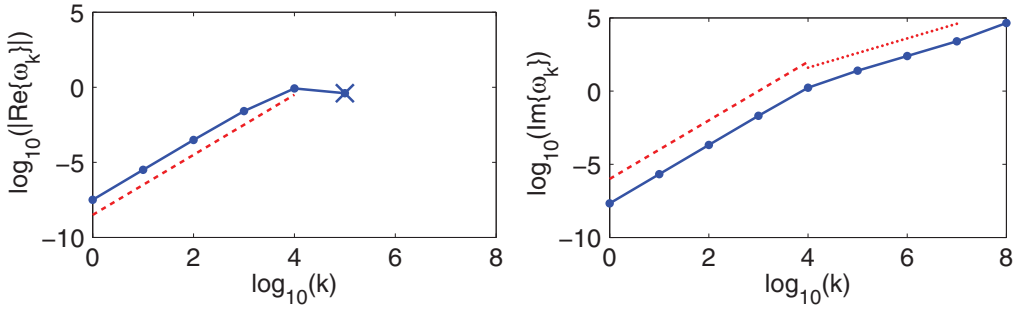

FIG. 3. (Color online) Real (left panel) and imaginary (right panel) parts of ω_k vs k for the purely viscous lipid membrane-fictitious solvent system. We note that ω_k is measured in s^{-1} while k is measured in m^{-1}. The dashed and dotted lines have slopes 2 and 1, respectively, and are guides to the eye. In the limit $k \to 0$, both real and imaginary parts scale with k^2, while at large k values, dissipation within the membrane dominates, leading to pure exponential relaxation with $\mathrm{Im}(\omega_k) \sim k$ and $\mathrm{Re}(\omega_k) = 0$. Note that $\log[\mathrm{Re}(\omega_k)] \to -\infty$ in the $k > 10^5\ \mathrm{m}^{-1}$ regime, and hence these data are omitted from the plot.

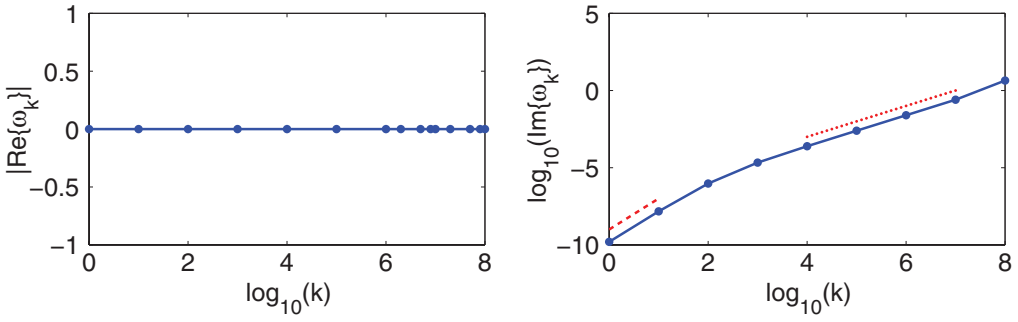

FIG. 4. (Color online) Real (left panel) and imaginary (right panel) parts of ω_k vs k for the viscoelastic lipid membrane-water solvent system. We note that ω_k is measured in s^{-1} while k is measured in m^{-1}. The dashed and dotted lines have slopes 2 and 1, respectively, and are guides to the eye. Notice how the fluctuation relaxation rate is dominated by membrane viscoelasticity for which $\omega_k \sim k$ with pure exponential relaxation over an extended range of k values for this choice of parameters.

IV. CONCLUSION

In this paper, we have presented a comprehensive analysis of compositional interface fluctuations in planar lipid bilayer membranes. Within the continuum phase-field framework, the starting point of our analysis was the advective Cahn-Hilliard equation, which governs the spatiotemporal evolution of the lipid composition in symmetric membranes, and which explicitly incorporates both advective and diffusive lipid transport processes. This equation in turn is coupled to the continuum hydrodynamic equations governing the flow behavior of the membrane and surrounding solvent with finite subphase thickness. In order to extract the interface dynamics from the continuum phase-field description, we first carried out a matched asymptotic expansion analysis in order to derive the so-called sharp-interface limit equations, which describe the compositional dynamics within bulk phases and assign specific boundary conditions along the moving interface.

Based on the sharp-interface limit equations, we then carried out a linear perturbation analysis for the dynamics of small-amplitude sinusoidal interface fluctuations to yield the general dispersion relation ω_k as a function of perturbation wave number k [cf. Eq. (22)], driven by compositional interfacial curvature and line tension. The resulting expression incorporates the effects of diffusive and advective lipid transport processes within the membrane, viscoelastic membrane properties, coupling between membrane and solvent, and inertial effects within the membrane and solvent with finite subphase thickness. As such, the general expression quantifies the decay of fluctuations over a broad range of length and time scales.

Having derived the expression for the general dispersion relation, we then demonstrated analytically that previously considered scenarios naturally emerge as limiting cases of our more general result. Furthermore, we considered two additional scenarios amenable to analysis, one in which the inertia of the solvent is relevant, and another one in which the membrane displays significant viscoelastic properties. Finally, we numerically evaluated the general dispersion relation for three representative model membrane systems. We are currently extending the analysis to investigate compositional interface fluctuations in asymmetric bilayer membranes.

ACKNOWLEDGMENTS

This work has been in part supported by an NSF-DMR Grant No. DMR-1006831. Useful discussions with Howard A. Stone are gratefully acknowledged.

APPENDIX: DERIVATION OF THE SHARP-INTERFACE LIMIT EQUATIONS FROM THE PHASE-FIELD APPROACH

Here we outline the derivation of the sharp-interface limit equations for the advective Cahn-Hilliard equation (1). As already alluded to in the main text, the challenge here is that the phase-field approach incorporates the presence of interfaces *implicitly*, rather than explicitly. In fact, the interfaces are located where the order parameter ψ varies rapidly yet smoothly from one compositional phase to another, and interfacial dynamics can be extracted from a perturbative analysis of solutions to Eq. (1) expanded around planar equilibrium (or steady-state) solutions. Furthermore, it will be assumed that (a) the interface is gently curved on the scale of the intrinsic interface width, (b) the normal velocity of the interface is sufficiently small to admit effectively instantaneous relaxation of the order parameter diffusion field within the diffuse interface, and (c) both the membrane and solvent are quiescent. In other words, the system is only slightly perturbed away from thermodynamic equilibrium.

The basic qualitative idea is as follows. We consider solutions to the governing equations in two distinct spatial regions, namely, regions in the vicinity of an interface ("inner region") and away from any interfaces ("outer region"). The governing equations in the outer region reduce to bulk equations, while matching the outer solutions to the inner ones within an overlap region provides the appropriate boundary conditions on the interface in the sharp-interface limit.

Technically, this procedure is carried out by means of matched asymptotic expansions, in which the small expansion parameter ϵ is related to the intrinsic interfacial width ξ and the velocity normal to the interface v_c via $\epsilon = \kappa_c \xi \sim \xi v_c / D_\psi \ll 1$, where D_ψ and κ_c denote the collective lipid diffusion coefficient and characteristic curvature of the interface, respectively. To facilitate the analysis, we first divide the spatial domain into two regions, namely the inner one, which is close to the

interface and wherein the fields vary rapidly over length scales $\sim O(\xi)$, and the outer one, which is far from any interfaces and wherein the fields vary over length scales $\sim O(\xi/\epsilon)$. To distinguish the inner and outer regions more clearly, it is useful to define an intermediate length scale ζ, which satisfies $1 \ll \zeta/\xi \ll 1/\epsilon$, and which corresponds to the overlap region. Below we will carry out asymptotic expansions in ϵ for both ψ and μ_ψ separately in the outer and inner regions, and then match them within the overlap region to yield the appropriate sharp-interface limit equations. For convenience, we use a curvilinear coordinate system (u,s) where u and s denote local coordinates perpendicular and parallel to the interface at $u \approx 0$, respectively, instead of the Cartesian one.

1. Inner region

In the inner region $(-\zeta < u < \zeta)$, we define $u = \xi\bar{u}$, $s = \xi\bar{s}/\epsilon$, and $\kappa = \epsilon\bar{\kappa}/\xi$. Following Ref. [20], we develop the following perturbation expansions in ϵ for the order parameter ψ, chemical potential μ_ψ, local interface velocity $\mathbf{v}$, membrane velocity $\mathbf{u}_M$, and spatiotemporal derivatives:

$$\psi = \psi_0^{\text{in}} + \epsilon\delta\psi_1^{\text{in}} + O(\epsilon^2), \tag{A1}$$

$$\mu_\psi = \mu_0^{\text{in}} + \epsilon\delta\mu_1^{\text{in}} + O(\epsilon^2), \tag{A2}$$

$$\mathbf{v} = \mathbf{v}_0^{\text{in}} + \epsilon\mathbf{v}_1^{\text{in}} + O(\epsilon^2), \tag{A3}$$

$$\mathbf{u}_M = \mathbf{u}_{M0}^{\text{in}} + \epsilon\mathbf{u}_{M1}^{\text{in}} + O(\epsilon^2), \tag{A4}$$

$$\xi\nabla = \mathbf{n}\frac{\partial}{\partial\bar{u}} + \epsilon\mathbf{t}\frac{\partial}{\partial\bar{s}} + O(\epsilon^2), \tag{A5}$$

$$\xi^2\nabla^2 = \frac{\partial}{\partial\bar{u}^2} + \epsilon\bar{\kappa}\frac{\partial}{\partial\bar{u}} + O(\epsilon^2), \tag{A6}$$

$$\left.\frac{\partial}{\partial t}\right|_{\mathbf{r}} = \left.\frac{\partial}{\partial t}\right|_{(u,s)} - \mathbf{v}\cdot\nabla = -\mathbf{v}\cdot\nabla + O(\epsilon^2). \tag{A7}$$

Here $\mathbf{n}$ ($\mathbf{t}$) denotes the unit vector perpendicular (parallel) to the interface located at $u \approx 0$, while κ denotes the local interface curvature. Note that $\mathbf{v}_0^{\text{in}} = \mathbf{u}_{M0}^{\text{in}} = 0$ due to the static equilibrium assumption, such that $\mathbf{v} \sim O(\epsilon)$ and $\mathbf{u}_M \sim O(\epsilon)$. (Of course, the expansions for ψ and μ_ψ are not independent, as $\mu_\psi = \delta F/\delta\psi$ by definition.) Also, note that we are working in the frame of reference where the interface is stationary, and where the term $\frac{\partial}{\partial t}|_{(u,s)} \sim O(\epsilon^2)$ arises from diffusive relaxation around the equilibrium state not accounted for by the motion of the interface.

Now, rewriting Eq. (1) in the inner region, it can be seen that the left-hand side becomes

$$\left.\frac{\partial\psi}{\partial t}\right|_{\mathbf{r}} + \mathbf{u}_M\cdot\nabla\psi = -\frac{\epsilon}{\xi}\left(\mathbf{v}_1^{\text{in}} - \mathbf{u}_{M1}^{\text{in}}\right)\cdot\mathbf{n}\frac{\partial\psi_0^{\text{in}}}{\partial\bar{u}} + O(\epsilon^2), \tag{A8}$$

while the right-hand side can be written

$$M\nabla^2\mu_\psi = \frac{M}{\xi^2}\frac{\partial^2\mu_0^{\text{in}}}{\partial\bar{u}^2} + \frac{\epsilon M}{\xi^2}\left(\bar{\kappa}\frac{\partial\mu_0^{\text{in}}}{\partial\bar{u}} + \frac{\partial^2\delta\mu_1^{\text{in}}}{\partial\bar{u}^2}\right) + O(\epsilon^2). \tag{A9}$$

Importantly, Eq. (A9) is exactly the same as in the Elder *et al.* analysis in Ref. [20], while Eq. (A8) differs from the one analyzed by Elder *et al.* only by the presence of the membrane velocity ($\mathbf{u}_{M1}$) term. Hence, in order to proceed, we need only to substitute $\mathbf{v}_1$ with $\mathbf{v}_1 - \mathbf{u}_{M1}$ and retrace the steps in their derivation. In fact, we can simply replace $\mathbf{v}$ with $\mathbf{v} - \mathbf{u}_M$ in their final results for the boundary conditions along the moving interface. However, in order to provide a reasonably self-contained exposition of the asymptotic analysis, below we outline the main steps in the derivation.

Upon collecting terms order by order in ϵ and carrying out the analysis procedure yields, at $O(\epsilon^0)$, the equilibrium solution for the planar interface, $\psi_0^{\text{in}}(\bar{u})$, which satisfies

$$2W^2\frac{d^2\psi_0^{\text{in}}(\bar{u})}{d\bar{u}^2} - \frac{df}{d\psi_0^{\text{in}}} = \mu_0^{\text{in}} = \mu_{\text{eq}}. \tag{A10}$$

Furthermore, at order $O(\epsilon)$, the following relations are obtained:

$$v_{1;n}^{\text{in}}\big|_{\text{int}} - u_{M1;n}^{\text{in}}\big|_{\text{int}} = -\frac{M}{\Delta\psi_{\text{eq}}\xi}\left(\left.\frac{\partial\delta\mu_1^{\text{in}}}{\partial\bar{u}}\right|_{\bar{\zeta}} - \left.\frac{\partial\delta\mu_1^{\text{in}}}{\partial\bar{u}}\right|_{-\bar{\zeta}}\right) \tag{A11}$$

and

$$\begin{aligned}
&\Delta\psi_{\text{eq}}\delta\mu_1^{\text{in}}(\pm\bar{\zeta},\bar{s}) \\
&= -\frac{\sigma\bar{\kappa}}{\xi} \pm \Delta\psi_{\text{eq}}\bar{\zeta}\left.\frac{\partial\delta\mu_1^{\text{in}}}{\partial\bar{u}}\right|_{\pm\bar{\zeta}} - \frac{\left(v_{1;n}^{\text{in}}\big|_{\text{int}} - u_{M1;n}^{\text{in}}\big|_{\text{int}}\right)\xi}{M} \\
&\quad\times\int_{-\infty}^{\infty} d\bar{u}\left[\psi_0^{\text{in}}(\bar{u}) - \psi_0^{\text{out}}(\bar{u})\right]^2 \\
&\quad - \left.\frac{\partial\delta\mu_1^{\text{in}}}{\partial\bar{u}}\right|_{-\bar{\zeta}}\int_{-\infty}^{0} d\bar{u}\left[\psi_0^{\text{out}}(\bar{u}) - \psi_0^{\text{in}}(\bar{u})\right] \\
&\quad - \left.\frac{\partial\delta\mu_1^{\text{in}}}{\partial\bar{u}}\right|_{\bar{\zeta}}\int_{0}^{+\infty} d\bar{u}\left[\psi_0^{\text{out}}(\bar{u}) - \psi_0^{\text{in}}(\bar{u})\right] \\
&\quad + \Delta\psi_{\text{eq}}\frac{\left(v_{1;n}^{\text{in}}\big|_{\text{int}} - u_{M1;n}^{\text{in}}\big|_{\text{int}}\right)\xi}{M} \\
&\quad\times\int_{0}^{\pm\infty} d\bar{u}\left[\psi_0^{\text{out}}(\bar{u}) - \psi_0^{\text{in}}(\bar{u})\right],
\end{aligned} \tag{A12}$$

where $\Delta\psi_{\text{eq}} = \psi_0^{\text{in}}(\bar{\zeta}) - \psi_0^{\text{in}}(-\bar{\zeta})$ denotes the miscibility gap, $\sigma \equiv 2W^2\int_{-\zeta}^{\zeta} du(\partial\psi_0^{\text{in}}/\partial u)^2$ is the line tension, $v_{1;n}^{\text{in}}|_{\text{int}}$ and $u_{M1;n}^{\text{in}}|_{\text{int}}$ denote the normal components of interface velocity and membrane velocity at the interface at order $O(\epsilon)$, respectively, $\pm\bar{\zeta} = \pm\zeta/\xi$ with $\bar{\zeta} \gg 1$, and

$$\psi_0^{\text{out}}(\bar{u}) = \begin{cases} \psi_0^{\text{in}}(-\bar{\zeta}) = \psi_{\text{eq}}^-, & \bar{u} < 0 \\ \psi_0^{\text{in}}(+\bar{\zeta}) = \psi_{\text{eq}}^+, & \bar{u} > 0. \end{cases} \tag{A13}$$

Equation (A11) relates the local interface velocity to the gradients in the local excess chemical potential on either side of the interface, while Eq. (A12) will be employed below to relate the local excess chemical at the interface to local interface curvature and velocity.

2. Outer region

In the outer region, variations of the fields take place on length scales $\sim O(\xi/\epsilon)$, so we define $u = \xi\tilde{u}/\epsilon$, $s = \xi\tilde{s}/\epsilon$, and $t = \tau_c\tilde{t}/\epsilon^2$. Again, upon carrying out the formal expansion in

ϵ, we can write

$$\psi^{\text{out}} = \psi_0^{\text{out}} + \epsilon\delta\psi_1^{\text{out}} + O(\epsilon^2), \tag{A14}$$

$$\mu_\psi^{\text{out}} = \mu_0^{\text{out}} + \epsilon\delta\mu_1^{\text{out}} + O(\epsilon^2), \tag{A15}$$

$$\mathbf{u}_M^{\text{out}} = \mathbf{u}_{M0}^{\text{out}} + \epsilon\mathbf{u}_{M1}^{\text{out}} + O(\epsilon^2), \tag{A16}$$

$$\xi\nabla = \epsilon\tilde{\nabla}, \tag{A17}$$

$$\frac{\partial}{\partial t} = \frac{\epsilon^2}{\tau_c}\frac{\partial}{\partial\tilde{t}}\ , \tag{A18}$$

where $\mathbf{u}_{M0}^{\text{out}} = 0$ again because of the static equilibrium assumption; thus, $\mathbf{u}_M^{\text{out}} \sim O(\epsilon)$.

Following the analysis strategy for the inner expansion, we then substitute the above expansions into Eq. (1), and collect terms order by order in ϵ. In this case, nontrivial results are first obtained at $O(\epsilon^2)$, which yield the bulk equilibrium solutions $\psi_0^{\text{out}} = \psi_{\text{eq}}^{\pm}$ for the two coexisting phases, and the equilibrium chemical potential $\mu_0^{\text{out}} = \mu_{\text{eq}}$. At $O(\epsilon^3)$, we obtain

$$\frac{\partial\delta\psi_1^{\text{out}}}{\partial t} + \mathbf{u}_{M1}\cdot\nabla\delta\psi_1^{\text{out}} = M\nabla^2\delta\mu_1^{\text{out}}, \tag{A19}$$

or, equivalently,

$$\frac{\partial\delta\psi}{\partial t} + \mathbf{u}_M\cdot\nabla\delta\psi = D_\psi\nabla^2\delta\psi, \tag{A20}$$

where $D_\psi \equiv M\frac{\partial\mu_\psi}{\partial\psi}|_{\psi_{\text{eq}}}$ denotes the diffusivity, and $\delta\psi = \psi^{\text{out}} - \psi_{\text{eq}}^{\pm}$ denotes the leading order deviation of the order parameter from the local bulk equilibrium value. It is noteworthy that the governing equation in the bulk region Eq. (A20) can also be obtained by simply linearizing Eq. (1) around the bulk equilibrium solution.

3. Matching

After carrying out the asymptotic expansions in both the inner and outer regions, we can finally match the solutions in the overlap region in order to obtain the appropriate boundary conditions at the interface. As in Ref. [20], the two matching conditions we exploit are (1) $\delta\mu_1^{\text{out}}(\tilde{u},\tilde{s}) = \delta\mu_1^{\text{in}}(\bar{u},\bar{s})$ and (2) $\partial\delta\mu_1^{\text{out}}(\tilde{u},\tilde{s})/\partial\tilde{u} = \partial\delta\mu_1^{\text{in}}(\bar{u},\bar{s})/\partial\bar{u}$, where $\tilde{u} = \epsilon\bar{u}$ and $\tilde{s} = \bar{s}$, and the matching is done at $\bar{u} = \pm\bar{\zeta}$. Note that the matching conditions simply reflect the fact that $\delta\mu^{\text{in}}$ and $\delta\mu^{\text{out}}$ are exactly the same function expressed in different variables in the overlap region.

By using the two matching conditions from above, we first employ the Taylor series expansion $\delta\mu_1^{\text{out}}(0,\tilde{s}) = \delta\mu_1^{\text{out}}(\pm\tilde{\zeta},\tilde{s}) \mp \tilde{\zeta}\,\partial\delta\mu_1^{\text{out}}/\partial\tilde{u}|_{\pm\tilde{\zeta}} + \cdots$ and the definition of the Gibbs dividing surface $\int_{-\infty}^{\infty} du[\psi_0^{\text{out}}(u) - \psi_0^{\text{in}}(u)] = 0$ to express Eqs. (A11) and (A12) in terms of $\delta\mu_1^{\text{out}}(0,\tilde{s})$ and $\partial\delta\mu_1^{\text{out}}/\partial\tilde{u}|_{(0,\tilde{s})}$. Then, after a few straightforward algebraic manipulations, we obtain the following set of sharp-interface limit equations, namely, (1) the bulk equation

$$\frac{\partial\delta\psi}{\partial t} + \mathbf{u}_M\cdot\nabla\delta\psi = D_\psi\nabla^2\delta\psi, \tag{A21}$$

and (2) the two boundary conditions along the interface, namely,

$$\frac{\delta\psi_{\text{int}}}{\Delta\psi_{\text{eq}}} = -d_0\kappa + \beta(v_n|_{\text{int}} - u_{Mn}|_{\text{int}}), \tag{A22}$$

from Eq. (A12), where $\beta \equiv \frac{1}{(\Delta\psi_{\text{eq}})^2 D_\psi}\int_{-\infty}^{\infty} du([\psi_0^{\text{out}}(u)]^2 - [\psi_0^{\text{in}}(u)]^2)$ denotes a kinetic undercooling coefficient, and

$$\Delta\psi_{\text{eq}}(v_n|_{\text{int}} - u_{Mn}|_{\text{int}}) = [D_\psi\nabla\delta\psi\cdot\mathbf{n}]_{0^+}^{0^-} \tag{A23}$$

from Eq. (A11). Finally, for systems close to equilibrium, the kinetic undercooling term can be neglected, and hence the appropriate boundary condition reduces to

$$\frac{\delta\psi_{\text{int}}}{\Delta\psi_{\text{eq}}} = -d_0\kappa. \tag{A24}$$

Equations (A21), (A23), and (A24) form the basis for the analysis of interface fluctuations employed in the main text.

[1] L. A. Bagatolli and E. Gratton, J. Fluoresc. **11**, 141 (2001).
[2] S. L. Veatch and S. L. Keller, Phys. Rev. Lett. **89**, 268101 (2002).
[3] P. Cicuta, S. L. Keller, and S. L. Veatch, J. Phys. Chem. B **111**, 3328 (2007).
[4] S. L. Veatch, P. Cicuta, P. Sengupta, A. R. Honerkamp-Smith, D. Holowka, and B. Baird, ACS Chem. Biol. **3**, 287 (2008).
[5] A. R. Honerkamp-Smith, S. L. Keller, and S. L. Veatch, Biochem. Biophys. Acta **1788**, 53 (2009).
[6] M. Haataja, Phys. Rev. E **80**, 020902 (2009).
[7] M. Laradji and P. B. Sunil Kumar, Phys. Rev. Lett. **93**, 198105 (2004).
[8] M. Laradji and P. B. Sunil Kumar, Phys. Rev. E **73**, 040901 (2006).
[9] S. Ramachandran, M. Laradji, and P. B. S. Kumar, J. Phys. Soc. Jpn. **78**, 041006 (2009).
[10] S. Ramachandran, S. Komura, and G. Gompper, Europhys. Lett. **89**, 56001 (2010).
[11] B. A. Camley and F. L. H. Brown, Phys. Rev. Lett. **105**, 148102 (2010).
[12] J. Fan, T. Han, and M. Haataja, J. Chem. Phys. **133**, 235101 (2010).
[13] E. Tüzel, G. Pan, and D. M. Kroll, J. Chem. Phys. **132**, 174701 (2010).
[14] E. G. Flekkoy and D. H. Rothman, Phys. Rev. E **53**, 1622 (1996).
[15] C. Esposito, A. Tian, S. Melamed, C. Johnson, S.-Y. Tee, and T. Baumgart, Biophys. J. **93**, 3169 (2007).
[16] E. K. Mann, S. Hénon, D. Langevin, and J. Meunier, Phys. Rev. E **51**, 5708 (1995).
[17] H. A. Stone and H. M. McConnell, Proc. R. Soc. Lond. A **448**, 97 (1995).
[18] B. A. Camley, C. Esposito, T. Baumgart, and F. L. H. Brown, Biophys. J. **99**, L44 (2010).
[19] B. A. Camley and F. L. H. Brown, Phys. Rev. E **84**, 021904 (2011).

[20] K. R. Elder, M. Grant, N. Provatas, and J. M. Kosterlitz, Phys. Rev. E **64**, 021604 (2001).
[21] D. Jasnow and J. Viñals, Phys. Fluids **8**, 660 (1996).
[22] P. C. Hohenberg and B. I. Halperin, Rev. Mod. Phys. **49**, 435 (1977).
[23] A. J. Levine and F. C. MacKintosh, Phys. Rev. E **66**, 061606 (2002).
[24] A. Serra and J. M. Rubí, Physica A **142**, 342 (1987).
[25] D. K. Lubensky and R. E. Goldstein, Phys. Fluids **8**, 843 (1996).
[26] N. Oppenheimer and H. Diamant, Phys. Rev. E **82**, 041912 (2010).
[27] H. A. Stone and A. Ajdari, J. Fluid Mech. **369**, 151 (1998).
[28] K. Seki, S. Ramachandran, and S. Komura, Phys. Rev. E **84**, 021905 (2011).
[29] T. Baumgart, S. T. Hess, and W. W. Webb, Nature (London) **425**, 821 (2003).
[30] W. H. Press, S. A. Teukolsky, W. T. Vetterling, and B. P. Flannery, *Numerical Recipes: The Art of Scientific Computing*, 3rd ed. (Cambridge University Press, New York, 2007).